Eur. Phys. J. D **9**, 517–521 (1999)

**THE EUROPEAN PHYSICAL JOURNAL D**

EDP Sciences
© Società Italiana di Fisica
Springer-Verlag 1999

# Structure of cobalt cluster films obtained by sputter deposition on alumina

J. Briático[1], J.-L. Maurice[1], J. Carrey[1], D. Imhoff[2], F. Petroff[1], and A. Vaurès[1]

[1] Unité Mixte de Physique CNRS/Thomson-CSF, Domaine de Corbeville, F-91404 Orsay, France
[2] Laboratoire de Physique de Solides, Université Paris-Sud, F-91405 Orsay, France

Received: 31 August 1998 / Received in final form: 22 October 1998

**Abstract.** We report on the structure of cobalt cluster films obtained by aggregation of metal atoms sputter-deposited on amorphous alumina. The cluster layers were encapsulated with a second amorphous alumina layer, also made by sputtering in the same chamber. Electron energy loss spectroscopy (EELS) indicates that encapsulation with sputtered alumina keeps the clusters free from cobalt oxide. Transmission electron microscopy (TEM) exhibits relatively narrow distributions of the cluster sizes and of the inter-cluster distances, which results in a noticeable local order. Size distributions appear quasi-Gaussian, but TEM misses an important number of small particles. Extended X-ray absorption fine structure (EXAFS) data shows that the actual average sizes are smaller, and Monte Carlo simulations suggest that the actual distributions could be bimodal, with a secondary peak in the small-size range.

**PACS.** 61.46.+w Clusters, nanoparticles, and nanocrystalline materials – 61.10.Ht X-ray absorption spectroscopy: EXAFS, NEXAFS, XANES, etc.

## 1 Introduction

Nanometer-sized metallic clusters are now being introduced in experimental electronic devices [1]. The insertion of a layer of cobalt aggregates in the insulator of a tunnel junction between magnetic electrodes combines giant magnetoresistance [2] with Coulomb blockade [3]. With these two effects, several types of future devices could be developed, such as microscopic magnetic reading heads or sensors and magnetically operated logic gates. We have used sputter deposition to prepare cobalt aggregates in alumina sandwiches. The alumina and metal layers were deposited sequentially, so that the formation of the cobalt aggregates was simply the result of the three-dimensional growth – the Volmer–Weber type – of a poorly wetting metal on an oxide. We have previously published the current perpendicular to the planes (CPP) transport properties of devices made of such films inserted between two ferromagnetic electrodes [2]. In the present article, we discuss some structural properties of these films, that we have studied by *ex situ* extended X-ray absorption fine structure (EXAFS), transmission electron microscopy (TEM), electron energy loss spectroscopy (EELS), and Monte Carlo simulation.

## 2 EXAFS measurements

Data collection was carried out at 77 K on the D42 station of the DCI storage ring (LURE) at the Co $K$ edge (7710 eV) using an Si(331) channel-cut monochromator. Detection of electrons was achieved by an ionization chamber filled with He gas.

Three different samples of alternating Co and $Al_2O_3$ layers were prepared by rf sputtering for this experiment, with a Co nominal thickness of 4, 7, and 30 Å, while the alumina nominal thickness was always 30 Å:

$$(\mathrm{Co} \times 4\,\text{Å}/\mathrm{Al_2O_3} \times 30\,\text{Å}) \times 70$$

$$(\mathrm{Co} \times 7\,\text{Å}/\mathrm{Al_2O_3} \times 30\,\text{Å}) \times 30$$

$$(\mathrm{Co} \times 30\,\text{Å}/\mathrm{Al_2O_3} \times 30\,\text{Å}) \times 10$$

Sputtering was achieved with 4-mTorr Ar plasma, and the substrate temperature was regulated at 293 K.

The EXAFS spectra of the samples and of a Co foil used as standard were recorded from 7600 eV to 8700 eV with a 2 eV step.

### 2.1 Data analysis

The X-ray absorption spectra were analyzed with standard procedures [4]. The oscillations were fitted with the Round Midnight program [5] in order to obtain the effective number of neighbors and their distances. Figure 1 shows the X-ray absorption spectrum, the extracted oscillations, the Fast Fourier Transform (FFT), and the Fourier-filtered oscillations, together with their fit, for the 30-Å Co sample.

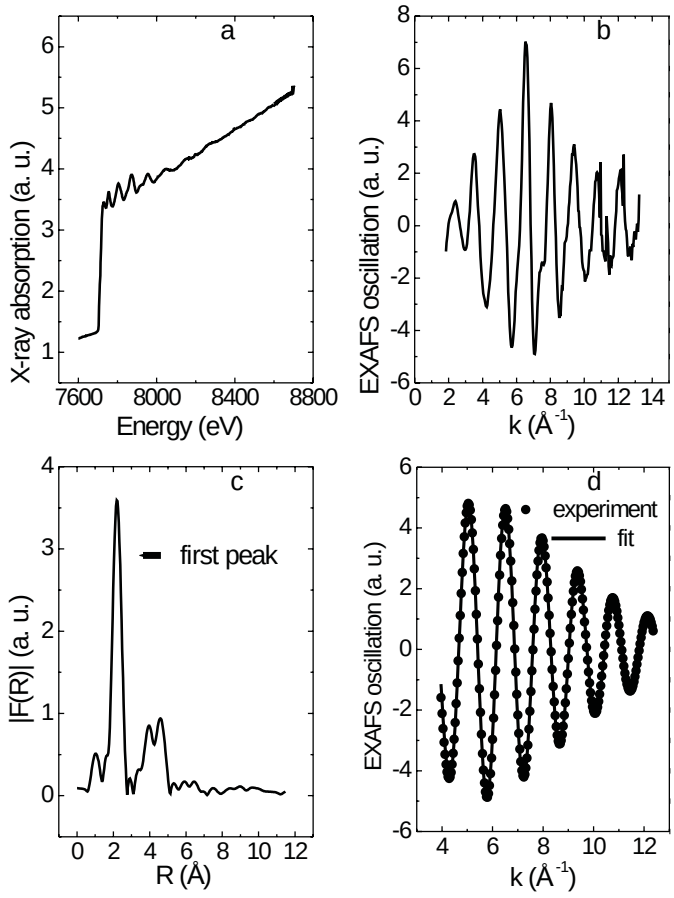


**Fig. 1.** Standard procedure for the EXAFS analysis: a) X-ray absorption spectrum; b) oscillations after background subtraction; c) FFT of the oscillations; d) fit to the oscillations after Fourier filtering.

### 2.2 EXAFS results

Table 1 shows the results obtained from the fit. The effective number of Co neighbors decreases when the nominal Co thickness is reduced. This reduction can be easily understood if we remember that Co forms aggregates in contact with $Al_2O_3$. Smaller thicknesses produce smaller aggregates. For large aggregates, we should find a number of neighbors close to that of bulk Co. For small aggregates, the ratio of bulk atoms to surface atoms is smaller, thus so is the effective number of pairs Co–Co. For this reason, oxygen atoms could be detected in the 4-Å nominal thickness sample.

To estimate the average aggregate diameter, we have simulated Co aggregates of different diameters. Then, we have computed the number of first neighbors of Co atoms for each aggregate, in order to construct a graph showing the number of first neighbors as a function of aggregate diameter (Fig. 2). By interpolating the effective number of neighbors obtained from EXAFS simulation in this graph, it is possible to obtain an EXAFS grain size, as shown in Table 1.

## 3 Transmission electron microscopy and EELS

Deposits composed of sandwiches of approximately 30-Å $Al_2O_3$/Co/30-Å $Al_2O_3$ were prepared for TEM on carbon membranes, with the Co nominal thickness varying between 2 and 50 Å. TEM and EELS were performed at 200 keV.

### 3.1 Assessment of the protecting layer

For the assessment of the protecting alumina layer, we have compared the images and the EELS spectra of two kinds of such layers, made over the same layer of Co clusters of 7 Å nominal thickness: a first one prepared with sputtered alumina (obtained from an alumina target), and a second one obtained with sputtered aluminium, oxidized afterwards, the latter having otherwise been recognized as a particularly good insulator [6]. The experimental TEM contrast of the clusters appears significantly larger in the former case. Two converging changes, in sample topography and in cluster chemical composition, happen to explain this. TEM image simulation shows that a bell-shaped covering, in the case of alumina, and a flat one, in the case of Al, already give some explanations to the observations [7]. But EELS indicates clear evidence of a chemical change (Fig. 3).

For the analysis of the EELS signal, we additionnaly recorded a spectrum from a metallic Co reference, composed of a 5-nm thick cobalt layer encapsulated in sputtered alumina. The Co–L near-edge fine structure in the first deposit (protected by sputtered alumina) is quite similar to that of the metallic reference (Fig. 3); this indicates that 3 nm of sputtered alumina efficiently protects the Co clusters against oxidation: Possible Co–O bonds, such as

**Table 1.** Results of the EXAFS fits: characteristics of Co clusters in layers with the nominal Co thickness indicated. The fit in the 4 Å case was best, with 0.86 oxygen first neighbors at 2.09 Å. See definition of the EXAFS grain size in text.

| Nominal thickness (Å) | Number/Type of first neighbors (bulk: 12) | EXAFS grain size (Å) | Distance to first neighbors (Å) (bulk: fcc: 2.5065 ; hcp: 2.505) |
|---|---|---|---|
| 4 | 6.93 / Co | 8.6 | 2.44 |
| | 0.86 / O | | 2.09 |
| 7 | 9.5 / Co | 19 | 2.481 |
| 30 | 11.7 / Co | >70 | 2.5067 |

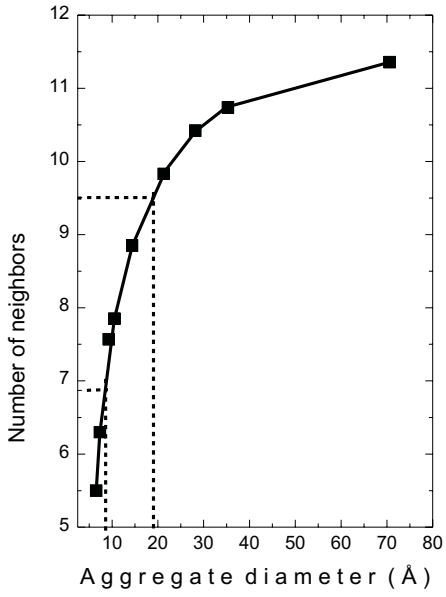


**Fig. 2.** Number of first neighbors vs. aggregate diameter for Co aggregates (see text above). Dashed lines indicate interpolation of the first neighbors number obtained from EXAFS experiments for the smallest samples.

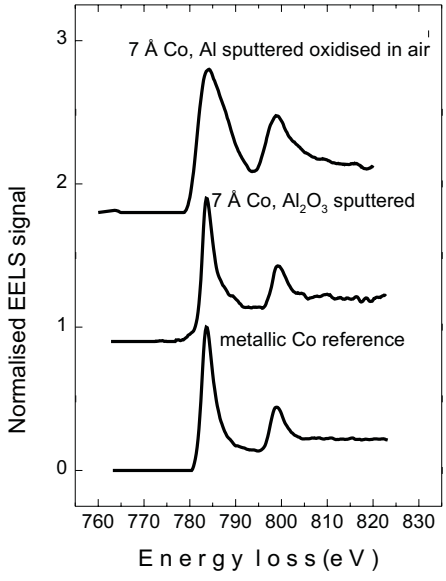


**Fig. 3.** EELS spectra recorded in the same operating conditions, after background subtraction: Co–L edge from a metallic Co reference (bottom), from the Co clusters protected by sputtered alumina (middle), and from the Co clusters protected by sputtered aluminium oxidized in air (top).

those detected by EXAFS, are too few to give a chemical signal. In contrast, the second deposit (sputtered Al) produces a noticeably different shape (Fig. 3). Although the origin of this difference is not obvious, the relatively greater importance of the L-2 peak suggests that it is due to the presence of a proportion of Co–O bonds. We thus used sputtered alumina for the protection of the cluster films discussed in the following.

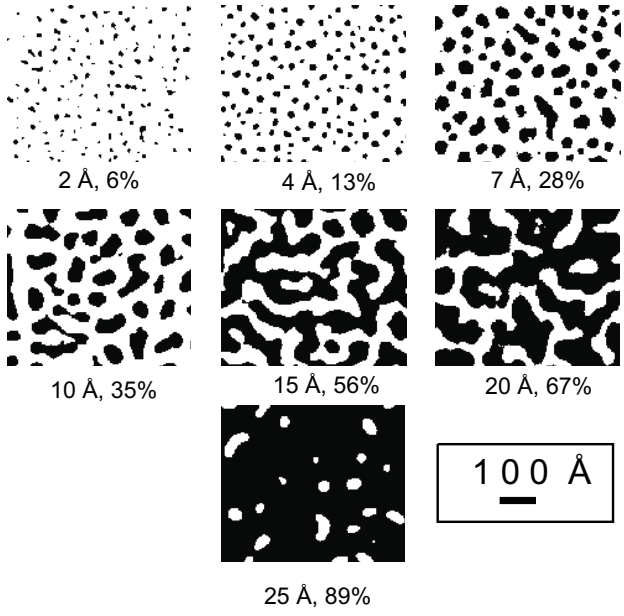


**Fig. 4.** Two-level TEM images of the Co deposits with the indicated nominal thicknesses. The respective coverages are also shown.

### 3.2 TEM images

The TEM images were digitized, filtered and binarized (Fig. 4), in order that the distributions of size and shape of the particles could finally be measured as a function of nominal thickness. As can be seen in Fig. 4, the whole range of thickness investigated lies in the coalescence regime, where the density of aggreates decreases as a function of nominal thickness. The results are summarized in Table 2.

However, that regime can be separated into three stages as a function of nominal thickness: (1) coalescence, keeping an almost spherical shape is kept [8]; (2) coalescence, giving a bean shape; and (3) coalescence above the percolation threshold. The nominal thicknesses planned were confirmed from the measure of the Co/Al ratio through the use of energy-dispersive X-ray spectroscopy (EDX); an exact nominal thickness of $Al_2O_3$ was supposed (Table 2) [9]. The significantly smaller nominal thicknesses deduced from the volume of the particles seen in the TEM [8] indicated the existence of a "hidden mass" not seen in the TEM that was probably composed of small clusters (see Table 2). The relative decrease of this hidden mass with increasing deposition time confirms that it lies in small particles.

## 4 Monte Carlo simulations

To simulate film growth, we used a modified version of the deposition diffusion aggregation (DDA) model [10]: at each step, the substrate receives a given density of atoms, and the atoms already on the surface are allowed to diffuse,

**Table 2.** Parameters of the deposits, deduced from the images in Fig. 4.

| Nominal thickness (Å) | EDX control (Å ± 5%) | Coverage ± 10% | Equivalent cluster diameter (Å ± 20%) | Density ($10^{12}$ cm$^{-2}$) | Deposited mass not seen by TEM |
|---|---|---|---|---|---|
| 2 | 2.01 | 6% | 8.3 | 9 | 89% |
| 4 | 4.09 | 13% | 14 | 7.7 | 77% |
| 7 | 6.65 | 28% | 28 | 4 | 45% |
| 10 | 10.7 | 35% | bean shape | 2 | 27% |
| 15 | 15.9 | 56% | – | 0.4 | – |
| 20 | 21.8 | 67% | percolation | – | 1% |
| 35 | – | 100% | – | – | 0% |

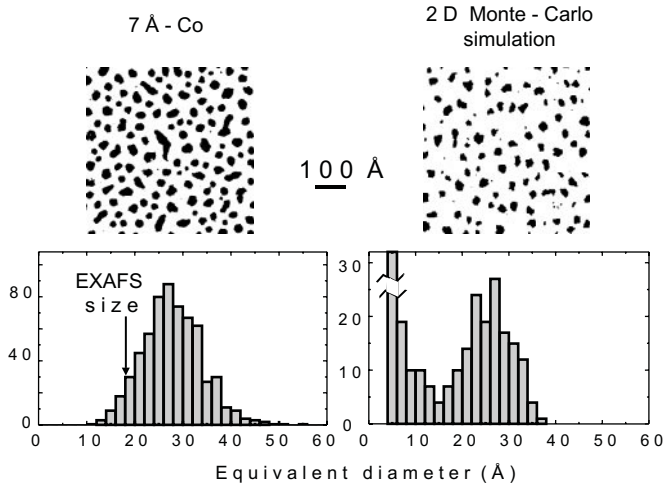


**Fig. 5.** Comparison between an experimental 7-Å deposit (left), and a 2D Monte Carlo simulated deposit (one pixel = one Co-atom) (right): images (top) and corresponding size histograms (bottom). The calculated deposit has been selected because it exhibits a similar size distribution for the larger sizes. Note the bimodal character of the distribution in that case, with a peak centered at 5 Å.

their probabilities of jump being calculated as a function of the number of their nearest neighbors [11]. These calculations are two-dimensional: one pixel is one Co atom, and an incoming atom falling on an existing cluster is not counted. Even though such a two-dimensional (2D) simulation can hardly reproduce the exact shape of a deposit, it allows one to draw useful general conclusions. Figure 5 thus compares the experimental image of the 7-Å cobalt deposit with a two-dimensional calculated deposit exhibiting the same dominant average cluster size. The histograms in Fig. 5 clearly show that the size distributions in the experimental and calculated cases are very similar for large sizes. The parameters used to obtain such a similarity correspond to a growth regime not far from the thermodynamic equilibrium: noticeable ripening and coalescence take place while the growth proceeds. However, there appears in the calculated deposit a second peak for small sizes. This second peak is centered on 5 Å, a size that corresponds to clusters of less than 10 atoms, particles definitely not detectable by TEM in the present experimental conditions. The simulations thus give an additional indication that the hidden part in our experimental deposits is composed of these small-size particles.

## 5 Discussion and conclusions

Although sputter deposition is often refered to as an out-of-equilibrium process, the shape of a given metal particle obtained on an oxide with this method can most often be described by the equilibrium of the surface tensions present [11].

The nonequilibrium part of the process shows in the size distribution of the particles. But even there, a quick look at the micrographs (Fig. 4) indicates that the distribution is quite homogeneous and that a Fourier transform of the images would indeed exhibit local order [8], as the inter-aggregate distance is almost constant over the film area. But, as shown in the above sections, the micrographs do not exhibit the whole aggregate population. The EXAFS analysis, which detects indistinctly all the Co atoms, indeed exhibits smaller grain sizes (Fig. 5). Although the real meaning of "EXAFS grain size" can be discussed, this unambiguously confirms the presence of out-of-equilibrium very small clusters. The histogram deduced from the simulated deposit in Fig. 5 exhibits a secondary peak in the small-size range, characteristic of these small particles. Annealing of these deposits so that an equilibrium state can be reached should thus desolve the smaller particles by Ostwald ripening and make the hidden mass progressively appear. This is difficult to realize with encapsulated cobalt, but we observed such an evolution with unencapsulated gold clusters annealed in air at room temperature [11].

We thank P. Jensen for giving us his code of the DDA program, and A. Traverse, D. Zanghi, P. Galtier, P. Seneor, J. Olivier, and A. Fert for fruitful discussion. We thank FOMEC (Argentina) and TMR program (CEE) for financial support.

## References

1. W. Chen, H. Ahmed: J. Vac. Sci. Technol. B **15**, 1402 (1997)
2. L.F. Schelp, A. Fert, F. Fettar, P. Holody, S.F. Lee, J.-L. Maurice, F. Petroff, A. Vaurès: Phys. Rev. B **56**, R5747 (1997)

3. R. Desmicht, G. Faini, V. Cros, A. Fert, F. Petroff, A. Vaurès: Appl. Phys. Lett. **72**, 386 (1998)
4. A. Traverse, S. Pizzini, S. Andrieu, A. Fontaine, M. Piecuch: Surf. Sci. **319**, 131 (1994)
5. A. Michalowizc: in *Logiciels pour la Chimie*, ed. by Société Française de Chimie, 1991, p. 102
6. J. Nassar, M. Hehn, A. Vaurès, F. Petroff, A. Fert: Appl. Phys. Lett. **73**, 698 (1998)
7. J. Briático, J.-L. Maurice, F. Petroff, P. Seneor, A. Vaurès, A. Fert: *Proceedings of the $14^{th}$ International Congress on Electron Microscopy*, Cancun, Mexico 1998
8. J.-L. Maurice, J. Briático, J. Carey, F. Petroff, A. Vaurès: to appear in Philos. Mag. A (1999)
9. F. Fettar, J.-L. Maurice, F. Petroff, L.F. Schelp, A. Vaurès, A. Fert: Thin Solid Films **319**, 120 (1998)
10. P. Jensen, A.-L. Barbasi, H. Larralde, S. Havlin, H.E. Stanley: Phys. Rev. B **50**, 15 316 (1994)
11. J.-L. Maurice, J. Carrey *et al.*: (in preparation)